Desalination and Water Treatment
www.deswater.com

doi: 10.1080/19443994.2013.846509

53 (2015) 689–696
January

Taylor & Francis
Taylor & Francis Group

Enhancement of TiO_2-UV100 nanoparticles photocatalytic activity by Mg impregnation in the removal of a model organic pollutant

Mohammad A. Behnajady*, Bahare Alizade

Faculty of Science, Department of Chemistry, Tabriz Branch, Islamic Azad University, Tabriz, Iran
Email: behnajady@iaut.ac.ir

Received 16 May 2012; Accepted 28 August 2013

ABSTRACT

In this study, Mg/TiO_2-UV100 nanoparticles were prepared by the impregnation method. The structural characteristics and properties of the obtained materials were investigated by X-ray diffraction (XRD), scanning electron microscopy, transmission electron microscopy (TEM), Brunauer–Emmett–Teller (BET) and diffuse reflectance spectroscopy (DRS) techniques. XRD patterns of pure and impregnated TiO_2-UV100 nanoparticles revealed that all phases were anatase. The results of BET analysis for Mg/TiO_2-UV100 nanoparticles indicated a surface area of 171.8 $m^2 g^{-1}$. Maximum distribution pore size is about 2 nm, which is consistent with microporous structure. The particle size obtained from TEM was close to crystallite size calculated from XRD pattern. A comparison of DRS of the Mg/TiO_2-UV100 with bare TiO_2-UV100 showed a slight red shift. The photocatalytic degradation of C.I. Acid Red 27 (AR27) was investigated in the presence of TiO_2-UV100 and Mg/TiO_2-UV100 nanoparticles under different conditions. The photocatalytic activity of Mg-impregnated (0.8 mol%) TiO_2-UV100 in the removal of AR27 was higher than that of bare TiO_2-UV100 nanoparticles. The photocatalytic activity of Mg-impregnated (0.8 mol%) TiO_2-UV100 was very sensitive to dopant content, initial concentration of the AR27, catalyst dosage, light intensity, and pH. The results indicated that the use of photocatalytic method in the presence of Mg-impregnated TiO_2-UV100 nanoparticles was a good choice for eliminating organic pollutants from aqueous media.

Keywords: Heterogeneous photocatalysis; Impregnation; TiO_2-UV100 nanoparticles; Magnesium; C.I. Acid Red 27

1. Introduction

The growing amount of industrial waste-containing refractory organic pollutants has entailed attempts to find new technologies for purifying the polluted water. One of the main modern technologies in this area has been the heterogeneous photocatalysis [1]. Ultraviolet irradiation on the semiconductor particles causes an excitation of electrons from valance band to the conduction band leading to the formation of holes in the valance band that are positively charged. Some species adsorbed on the surface of the semiconductor such as hydroxyl ions, water molecules, dissolved oxygen molecules and organic species get involved in redox reactions with photogenerated electrons and holes [2,3]. One of the important factors

*Corresponding author.

in photocatalytic efficiency is the competition between the ratio of the transfer of surface charge carrier and the electron-hole pair recombination. If the recombination process is too fast, other surface chemical operations do not occur [4]. Photocatalysis process has some shortcomings that limit its use in high-scale operations. For example, the rate of this process is limited by the low rate of the transfer of electrons to oxygen and more recombining of electron-hole pairs [5]. Moreover, the relatively wide band gap of semiconductors, such as TiO_2, practically limits the use of sunlight or visible light as a radiation source in photocatalysis process. To decrease the rate of electron-hole recombination in photocatalytic process and increase the amount of the absorption of solar spectrum, some efforts have been made [6,7]. Methods that have been used include semiconductor coupling [8–12], doping metal or non-metal ions at TiO_2 [13–18] and dye photosensitization on the TiO_2 surface [19–21]. The increase in the absorption of light and changing the capacities of TiO_2 into visible light is primarily affected by dopant [22]. It should be noted that further increase in dopant content exerts a negative effect on the activity of photocatalyst [23].

However, the TiO_2 doped with transition metals has some weaknesses including thermal instability and low quantum efficiency of the photoinduced charge carriers [24]. Among these metals, some of them like Ag are toxic. Magnesium is particularly suitable because of its low cost, easy preparation and nontoxicity. Feng et al. [25] prepared eight metal ions doped TiO_2 by an ultrasonic method and indicated the highest photocatalytic activity for Mg/TiO_2 under solar light. Venkatachalamet al. [26] have reported higher photocatalytic activity for magnesium and barium doped TiO_2 nanoparticles in comparison with bare TiO_2 in removing 4-chlorophenol. In this investigation, pure TiO_2 with anatase and rutile phases and ion-doped TiO_2 with pure anatase phase were synthesized by the sol–gel method. In other words, adding magnesium or barium hinders the crystallization of rutile phase of TiO_2 after calcination in a muffle furnace at 500°C for 5 h.

Among different commercially available titania powders, TiO_2–P25 (Degussa Co.) shows the highest activity in the majority of photocatalytic oxidation reactions. TiO_2–P25 consisting of a mixture of anatase and rutile in a proportion of 80/20% is characterized by a specific surface area of $50\,m^2\,g^{-1}$ and particle size of 21 nm. TiO_2-UV100 Hombikat is another commercial titania powder consisting of pure anatase phase. This commercial product is characterized by a specific surface area of $350\,m^2\,g^{-1}$ and particle size of 8 nm [27]. FTIR studies indicated that TiO_2-UV100, unlike TiO_2–P25, does not contain isolated hydroxyl groups [28,29]. Recently, Patil et al. [30] have reported higher photocatalytic activity for TiO_2-UV100 in comparison with TiO_2–P25 in photocatalytic degradation of Congo red. The higher surface area of TiO_2-UV100 compared with TiO_2–P25 ($\approx$ 7 times) indicates that it can be a suitable catalyst in the impregnation process for higher photoactivity.

This study aims to improve the photocatalytic activity of TiO_2-UV100 nanoparticles with a crystallite size of 8 nm by using surface modification with Mg. The photocatalytic activity of the modified catalyst was compared with pure TiO_2-UV100 nanoparticles in removing C.I. Acid Red 27 (AR27) as a modal contaminant from textile industry. Various reaction parameters such as the effect of Mg-doping content, AR27 concentration, TiO_2-UV100 dosage and light intensity on the photocatalytic activity have been investigated.

2. The experiment

2.1. Materials

The titanium dioxide sample used in all experiments was TiO_2-UV100 Hombikat from Sachtleben Chemie-Germany. Magnesium nitrate was used from Scharlau Co., and C.I. Acid Red 27 (AR27), a mono-azo-anionic dye, was obtained from Merck. Its chemical structure and other characteristics are listed in Table 1.

2.2. Catalyst preparation

Magnesium-impregnated TiO_2-UV100 was prepared in the following way: TiO_2-UV100 was dispersed in distilled water, and then, a concentration of magnesium nitrate was added to the calculated amount of TiO_2 to obtain a dopant concentration within the range of 0–1% mol. The solution prepared in this way was placed in ultrasonic batch for 15 min and refluxed at 80°C for 4 h. Afterwards, the precipitate was washed and dried at 80°C for 10 h and calcined at 350°C for 1 h.

2.3. The characterization of the obtained nanoparticles

The crystalline phase and crystallite size of TiO_2-UV100 nanoparticles (bare and impregnated) were analyzed by X-ray diffraction (XRD) measurements that were carried out at room temperature by using Siemens XRD D5000 with Cu Kα radiation as the X-ray source. The average crystallite size (D) was calculated using Scherrer's equation:

Table 1
Chemical structure and characteristics of C.I. Acid Red 27

Structure			
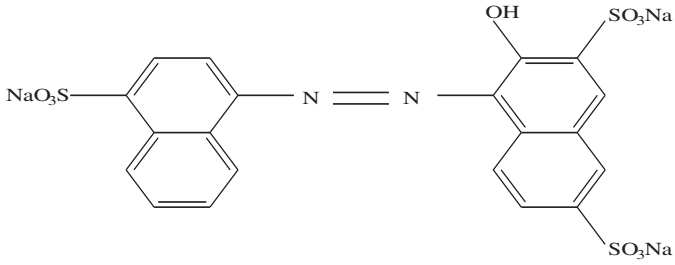			
Other names Amaranth, Azorubin S, FD & C Red 2, Food Red 9			Molecular formula $C_{20}H_{11}N_2Na_3O_{10}S_3$
Molecular mass ($g\,mol^{-1}$) 604.48	Absorption maximum (nm) 522	Colour index no. 16,185	Appearance Dark red solid

$$D = \frac{k\lambda}{\beta \cos\theta}$$

where k is the shape factor (0.89), λ is the X-ray wavelength (0.154056 nm), β is the full width at half-maximum of the diffraction line, and θ is the diffraction angle. Diffuse reflectance spectroscopy (DRS) of photocatalysts was obtained using Avaspec 2048 TEC as spectrometer. The surface morphology was analyzed by scanning electron microscopy (SEM) technique (Tescan Vegal). SEM was equipped with an EDX system. The size of nanoparticles was observed using transmission electronic microscopy (Philips CM-10 HT-100 keV). The specific surface area, total pore volume, and the mean pore diameter of the impregnated sample were determined by Brunauer–Emmett–Teller (BET) and Barratt–Joyner–Halenda (BJH) methods. Photocatalytic degradation of the model contaminant (AR27) was carried out in a bath quartz photoreactor of 100 mL volume. The light source was a visible light (300 W, 98% wavelength greater than 400 nm, manufactured by Osram) in vertical array with tubular quartz reactor. Light intensity was measured by Lux-UV–IR meter (Leybold Co.), and variation in the distance between radiation source and quartz photoreactor caused changes in light intensity.

2.4. Procedures

For photocatalytic degradation of AR27, in each experiment, 100 mL of the dye solution (containing AR27 and Mg/TiO_2-UV100 or TiO_2-UV100 nanoparticles) was used. The solution was kept in the darkness for 30 min. Oxygen was bubbled through the reactor with 0.5 mL min^{-1} flow rate. To maintain the homogeneity of the solution, O_2 flow was maintained in the photoreactor. After 30 min, when the lamp was turned on, the reaction was initiated, and at certain time intervals, 5 mL of the sample was withdrawn and analyzed with a UV–Vis spectrophotometer (Ultrospec 2000, Biotech Pharmacia, England). Total organic carbon (TOC) measurements were carried out by TOC analyzer (Shimadzu TOC-V_{csn}).

3. Results and discussion

3.1. The characterization of the photocatalyst

3.1.1. XRD measurement

Based on XRD patterns (Fig. 1), the crystallite size and phase composition of pure and Mg/TiO_2-UV100

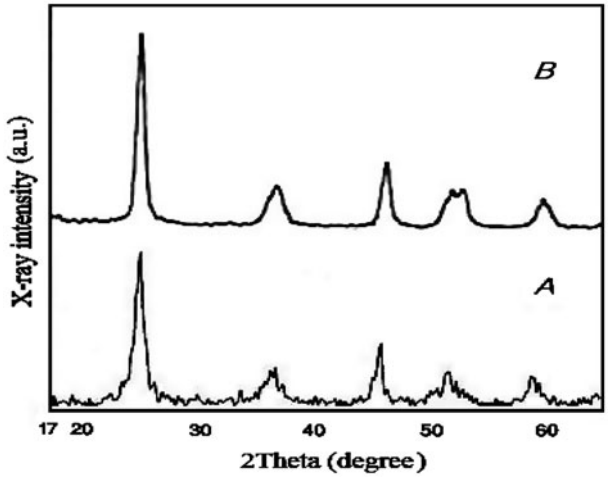

Fig. 1. XRD patterns of (A) bare TiO_2-UV100, (B) 0.8 mol% Mg/TiO_2-UV100 nanoparticles.

Table 2
XRD, BET, and BJH analysis results for TiO_2-UV100 and 0.8 mol% Mg/TiO_2-UV100 nanoparticles

Catalyst	TiO_2-UV100	0.8 mol% Mg/TiO_2-UV100
Anatase (A)/Rutile (R) ratio	100% (A)	100% (A)
Crystallite size (nm)	8	10
Surface area (m^2/g)	350.81	171.85
Most distribution pore size (nm)	1.21	2.10
Mean pore diameter (nm)	5.99	10.37
Total pore volume ($cm^3\,g^{-1}$)	0.5255	0.4455

nanoparticles are reported in Table 2. The major crystallite peak in the XRD patterns of TiO_2-UV100 and Mg/TiO_2-UV100 was anatase without any impurity peak as for Mg or rutile phase. This is probably attributed to low Mg content as well as appropriate dispersion of impregnated ion onto TiO_2-UV100 nanoparticles [31]. The characteristic peak of anatase phase at $2\theta \approx 25.4^\circ$ becomes stronger and sharper under Mg impregnation process.

3.1.2. TEM analysis

The transmission electron microscopy (TEM) image of Mg/TiO_2-UV100 nanoparticles is shown in Fig. 2. The bright gray particles in the micrograph are titania. It can be seen that the prepared sample has agglomerated to larger particles. However, the average particle size of the Mg/TiO_2-UV100 nanoparticles is close to the crystallite size calculated from the XRD pattern.

3.1.3. SEM–EDX analysis

Besides the crystallite size and phase composition, morphology is another important factor that determines the quality of a powder and its usefulness when being used. Therefore, SEM was used to investigate the morphology of Mg/TiO_2-UV100 nanoparticles (Fig. 3). As shown in SEM image, Mg/TiO_2-UV100 nanoparticles tend to form large agglomerates. This result is in agreement with the findings of other studies indicating that the particles with smaller grain size have higher tendency for agglomeration [32].

EDX analysis was carried out for Mg/TiO_2-UV100 nanoparticles to identify the elements present in an impregnated sample. Fig. 4 shows the EDX result for 0.8 mol% Mg/TiO_2-UV100 nanoparticles. The analytical results from EDX are in reasonable agreement with the experimental value of Mg impregnated onto TiO_2-UV100 nanoparticles.

3.1.4. DRS analysis

Fig. 5 shows the DRS of the Mg/TiO_2-UV100 and bare TiO_2-UV100 nanoparticles. The spectrum of the Mg-impregnated sample in Fig. 5 shows a slight red shift in the band-gap transition to longer wavelengths. The absorption edge cutoff was obtained by extrapolating the linear region of the DRS to zero. Bare TiO_2-UV100 shows the absorption edge cutoff around 392 nm, while Mg-impregnated TiO_2-UV100 shows the absorption edge cutoff around 402 nm. It is

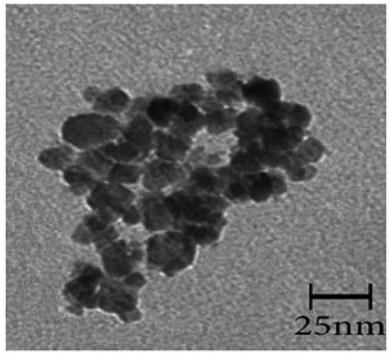

Fig. 2. TEM image of the 0.8 mol% Mg/TiO_2-UV100 nano particles.

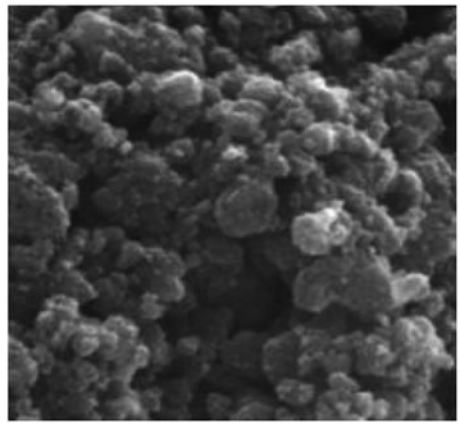

Fig. 3. SEM micrograph of 0.8 mol% Mg/TiO_2-UV100 nano particles.

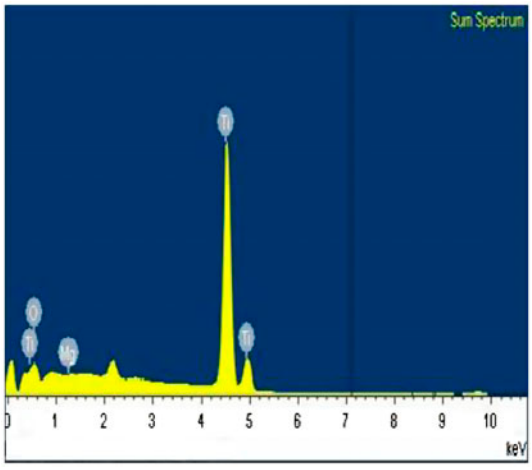

Fig. 4. EDX spectra of 0.8 mol% Mg/TiO_2-UV100 nano particles.

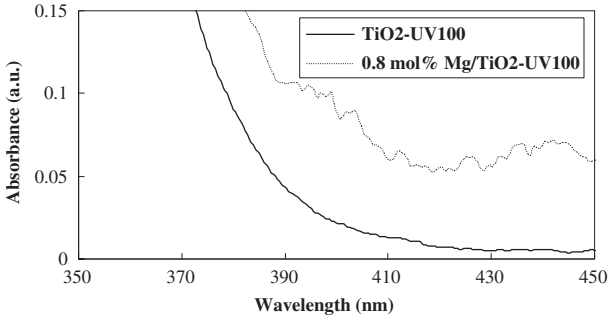

Fig. 5. DRS of bare TiO_2-UV100 and 0.8 mol% Mg/TiO_2-UV100 nanoparticles.

expected to observe higher photocatalytic activity for Mg-impregnated TiO_2-UV100 in comparison with bare TiO_2 under visible light irradiation, because Mg-impregnated TiO_2-UV100 absorbs light in wider wavelengths. The band-gap value of doped sample can be related to the crystallite size and defect concentration. It was observed that the sample with larger crystallite size and higher defect concentration showed smaller amount of band-gap value [33].

3.1.5. BET analysis

Fig. 6 presents N_2 adsorption/desorption isotherms and BJH pore size distribution curve (inset) of 0.8 mol% Mg-impregnated TiO_2-UV100 nanoparticles calcined at 350°C for 1 h. Results obtained from BET and BJH methods are reported in Table 2. According to IUPAC classification, Mg-impregnated TiO_2-UV100 nanoparticles display a Type-III isotherm. BET surface area was 171.85 $m^2 g^{-1}$. The pore size distribution from the adsorption branch was determined by the

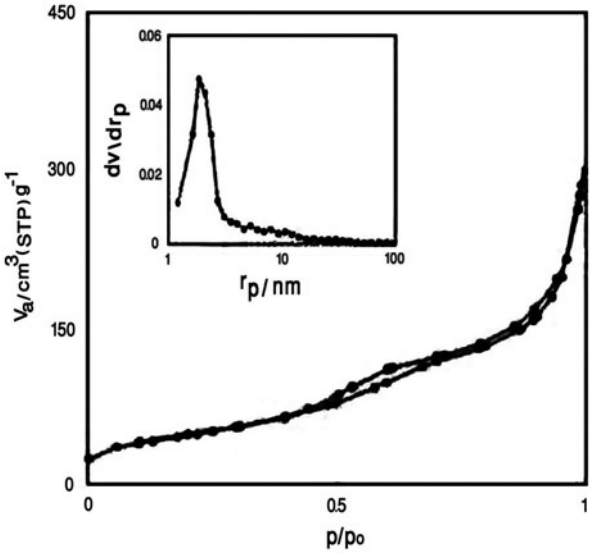

Fig. 6. The N_2 adsorption/desorption isotherm and BJH pore size distribution curve (inset) of 0.8 mol% Mg/TiO_2-UV100 nanoparticles.

BJH method. As shown in the inset in Fig. 6, the most distribution pore size is about 2 nm, which is consistent with the microporous structure.

3.2. Photocatalytic activity studies

3.2.1. The effect of Mg doping content

Photolysis of AR27 under UV irradiation alone has a negligible effect on the removal of AR27. Also, due to proximity of the natural pH of the solution to TiO_2-UV100 pH_{zpc}, adsorption of AR27 onto TiO_2 surface was low. The photocatalytic oxidation kinetics of many organic compounds has often been modeled with the modified Langmuir–Hinshelwood equation [34] as Eq. (1):

$$R = -\frac{d[AR27]}{dt} = \frac{k_{L-H}K_{ads}[AR27]}{1 + K_{ads}[AR27]_0} = k_{ap}[AR27] \quad (1)$$

and

$$k_{ap} = \frac{k_{L-H}K_{ads}}{1 + K_{ads}[AR27]_0} \quad (2)$$

where R is the reaction rate (mg L^{-1} min^{-1}), k_{L-H} is the reaction rate constant (mg L^{-1} min^{-1}), K_{ads} is the adsorption coefficient of AR27 on the TiO_2 particles (mg^{-1} L), [AR27] is the concentration of AR27 (mg L^{-1}), and $[AR27]_0$ is the initial concentration of AR27 (mg L^{-1}). Eq. (1) shows a pseudo-first-order reaction with respect to AR27 concentration. By integrating Eq. (1), the following equation is obtained:

$$\ln\frac{[AR27]_0}{[AR27]} = k_{ap}t \quad (3)$$

The semi-logarithmic graphs of the AR27 concentration in the presence of various photocatalysts vs. visible light irradiation time yield straight lines that confirm the pseudo-first-order kinetics for the removal of AR27 in this process. The apparent reaction rate constants (k_{ap}) for the photocatalytic removal of AR27 were obtained from the slope of the semi-logarithmic graphs.

The change in the photocatalytic activity of TiO_2-UV100 nanoparticles by impregnation method with various contents of Mg ions is shown in Fig. 7. The results in Fig. 7 show that Mg loading on TiO_2-UV100 surface has an optimum value of 0.8 mol % in the removal of AR27. As it can be seen, the k_{ap} increased with an increase in the Mg loading up to optimum loading point and then decreased. The Mg loaded on TiO_2 particles may create a space charge layer separating the photo-induced electron-hole pairs. With increasing Mg loading, the barrier on the surface gets higher, and the large electric fields separate the electron-hole pairs, but the excess Mg on the surface of TiO_2 screens the TiO_2 surface from light leading to low photoactivity [35].

3.2.2. The effect of catalyst dosage

Fig. 8 shows the variation of k_{ap} vs. 0.8 mol% Mg-impregnated TiO_2-UV100 nanoparticles dosage. The results indicate that the photocatalytic removal rate increases with catalyst loading until 800 mg L^{-1} and then decreases at high values due to light scattering and screening effects. Higher dosages of the solids cause higher agglomeration (particle/particle interaction); this reduces the available surface area for absorbing the light and also adsorbing AR27 molecules. Therefore, although with the rise of catalyst loading, the active sites of the catalyst increases, photocatalytic activity decreases due to light scattering in higher dosages [36].

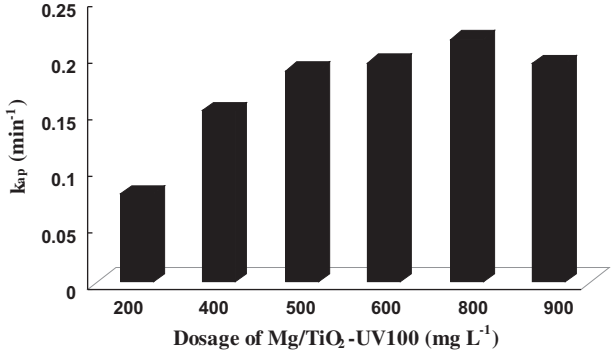

Fig. 8. Effect of various dosages of 0.8 mol% Mg/TiO_2-UV100 nanoparticles at degradation of AR27. $I_o = 190$ klx, $[AR27]_o = 33 \times 10^{-3}$ mM.

3.2.3. The effect of initial concentration of AR27

After optimizing the catalyst dosage, the photocatalytic removal of AR27 was carried out by varying the initial concentration of AR27. The influence of initial AR27 concentration within the range of 33×10^{-3}–66×10^{-3} mM on the removal rate was studied in the presence of 0.8 mol% Mg-impregnated TiO_2 (Fig. 9). It is generally noted that the degradation rate decreases with increase in pollutant concentration. This may be justified with the fact that high absorption coefficient of AR27 in UV-vis regions in higher initial concentrations causes an inner filter effect. On the other hand, in high AR27 initial concentrations, more organic substances are adsorbed on the surface of catalyst, and consequently, the amount of hydroxyl radicals and photocatalytic activity decrease [27].

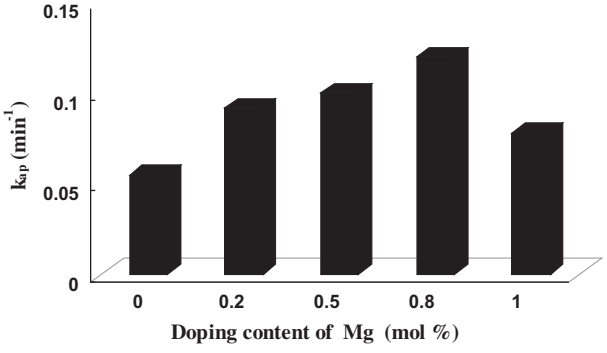

Fig. 7. Effect of Mg content on the photoactivity of Mg/TiO_2-UV100 nanoparticles at degradation of AR27. $I_o = 190$ klx, $[AR27]_o = 33 \times 10^{-3}$ mM, [Mg/TiO_2-UV100] = 400 mg L^{-1}.

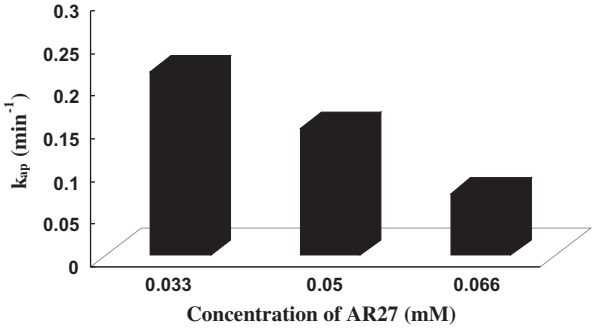

Fig. 9. Effect of the initial AR27 concentration on the photoactivity of 0.8 mol% Mg/TiO_2-UV100 nanoparticles at degradation of AR27. $I_o = 190$ klx, [0.8 mol% Mg/TiO_2-UV100] = 800 mg L^{-1}.

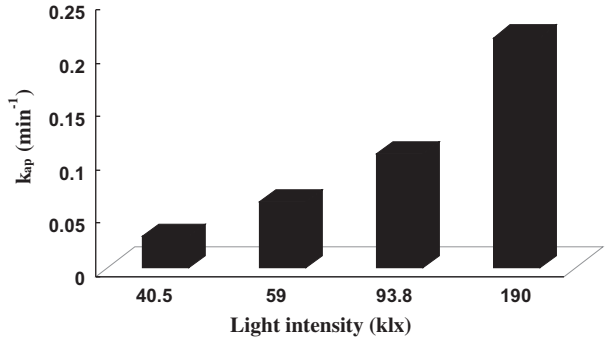

Fig. 10. Effect of the light intensity on the photoactivity of 0.8 mol% Mg/TiO_2-UV100 nanoparticles at degradation of AR27. $[AR27]_o = 33 \times 10^{-3}$ mM, [0.8 mol% Mg/TiO_2-UV100] = 800 mg L^{-1}.

3.2.4. The effect of light intensity

Fig. 10 shows the effect of light intensity on the removal of AR27 in the presence of 0.8 mol%-Mg-impregnated TiO_2-UV100 nanoparticles. With increasing light intensity from 40.5 to 190 klx, the percentage of degradation increases from 10 to 98% at 30-min radiation time. Under higher light intensities, the catalyst absorbs more photons. Therefore, the more electron-hole pairs and hydroxyl radicals will be formed. In lower light intensity, there is a competition between electron-hole recombination and consumption leading to less creation of hydroxyl radicals [37]. Mineralization of the pollutant was monitored through TOC measurement under 190 klx light intensity. The results of mineralization study indicated that 81% TOC reduction of AR27 with an initial concentration of 33×10^{-3} mM is possible in the presence of 0.8 mol% Mg-impregnated TiO_2-UV100 nanoparticles after 60 min irradiation.

3.2.5. The effect of pH

An important parameter governing the photocatalytic activity of TiO_2 is the pH of the dispersions. Due to amphoteric behavior of TiO_2, pH influences the surface charge of metal oxide and also ionization state of solute [38]. Experiments were carried out at pH values of 3, 5.4 (natural pH of solution) and 9, using 20 mg L^{-1} AR27 solutions along with 800 mg L^{-1} of 0.8 mol% Mg-impregnated TiO_2-UV100 nanoparticles under 190 klx light intensity.

The pH of zero point of charge (pH_{zpc}) represents surface charge of metal oxide at different initial pHs. The pH_{zpc} for TiO_2-UV100 nanoparticles is 6.2 [39]. When pH is lower than, 6.2 the positively charged surface sites on the TiO_2-UV100 nanoparticles increase. Interactions between AR27 molecules with anionic character and TiO_2-UV100 nanoparticles sites will be favored at low pH (< 6.2). The results of experiment at the pH = 3 indicates a considerable adsorption of AR27 onto the surface of the catalyst; therefore, a comparison of photocatalytic activity with other pHs is not possible. Blank experiment was also performed in the dark, confirming that significant adsorption of AR27 occurred at acidic conditions. The comparison between photocatalytic activity of 0.8 mol % Mg-impregnated TiO_2-UV100 nanoparticles at pHs of 5.4 (natural pH of solution) and 9 indicated that the enhancement of pH to alkaline pH causes the decrease of k_{ap} from 0.216 to 0.016 min^{-1}. The adsorption of AR27 at basic pH is prevented by repulsive electrostatic forces existing between AR27 molecules with anionic character and negatively charged surface sites that are predominant in this range of pH. Thus, decreased adsorption would result in a considerable decline in AR27 removal rate.

4. Conclusion

The TiO_2-UV100 nanoparticles with different Mg contents were prepared via impregnation method, and photocatalytic activity was investigated in the removal of AR27. The comparison of the bare TiO_2-UV100 and Mg-impregnated TiO_2-UV100 DRS indicated that the impregnated sample showed a slight red shift. The results of XRD indicated that the major phase of Mg-impregnated TiO_2-UV100 nanoparticles was anatase without any other peak corresponding to Mg. The SEM micrograph of Mg-impregnated TiO_2-UV100 nanoparticles showed aggregated particles. The BET and BJH graphs showed microporous structure with a narrow distribution of pore size. Increasing photocatalytic activity of TiO_2-UV100 in the removal of AR27 was made possible by increasing Mg content up to 0.8 mol%. The removal rate of AR27 in the presence of Mg-impregnated TiO_2 nanoparticles was a function of catalyst dosage, pollutant concentration, light intensity, and pH.

Acknowledgments

The authors would like to thank the financial support of the Islamic Azad University, Tabriz Branch, and the Iranian Nanotechnology Initiative Council.

References

[1] I. Oller, W. Gernjak, M.I. Maldonado, L.A. Perez-Estrada, J.A. Sanchez-Perez, S. Malato, Solar photocatalytic degradation of some hazardous water-soluble pesticides at pilot-plant scale, J. Hazard. Mater. 138 (2006) 507–517.

[2] V. Vamathevan, R. Amal, D. Beydoun, G. Low, S. McEvoy, Photocatalytic oxidation of organics in water using pure and silver-modified titanium dioxide particles, J. Photochem. Photobiol., A 148 (2002) 233–245.
[3] A. Nageswara Rao, B. Sivasankar, V. Sadasivam, Kinetic studies on the photocatalytic degradation of Direct Yellow 12 in the presence of ZnO catalyst, J. Mol. Catal. A: Chem. 306 (2009) 77–81.
[4] L. Gomathi Devi, N. Kottam, B. Narasimha Murthy, S. Girish Kumar, Enhanced photocatalytic activity of transition metal ions Mn^{2+}, Ni^{2+} and Zn^{2+} doped polycrystalline titania for the degradation of Aniline Blue under UV/solar light, J. Mol. Catal. A: Chem. 328 (2010) 44–52.
[5] S.X. Liu, Z.P. Qu, X.W. Han, C.L. Sun, A mechanism for enhanced photocatalytic activity of silver-loaded titanium dioxide, Catal. Today 93–95 (2004) 877–884.
[6] M.S. Lee, S.S. Hong, M. Mohseni, Synthesis of photocatalytic nanosized TiO_2–Ag particles with sol–gel method using reduction agent, J. Mol. Catal. A: Chem. 242 (2005) 135–140.
[7] M. El-Kemary, Y. Abdel-Moneam, M. Madkour, I. El-Mehasseb, Enhanced photocatalytic degradation of Safranin-O by heterogeneous nanoparticles for environmental applications, J. Lumin. 131 (2011) 570–576.
[8] Sh. Rehman, R. Ullah, A.M. Butt, N.D. Gohar, Strategies of making TiO_2 and ZnO visible light active, J. Hazard. Mater. 170 (2009) 560–569.
[9] Y. Bessekhouad, D. Robert, J.V. Weber, Bi_2S_3/TiO_2 and CdS/TiO_2 heterojunctions as an available configuration for photocatalytic degradation of organic pollutant, J. Photochem. Photobiol., A 163 (2004) 569–580.
[10] L. Wu, J.C. Yu, X. Fua, Characterization and photocatalytic mechanism of nanosized CdS coupled TiO_2 nanocrystals under visible light irradiation, J. Mol. Catal. A: Chem. 244 (2006) 25–32.
[11] W. Ho, J.C. Yu, Sonochemical synthesis and visible light photocatalytic behavior of CdSe and $CdSe/TiO_2$ nanoparticles, J. Mol. Catal. A: Chem. 247 (2006) 268–274.
[12] S. Ji, M.H. Jun, J.S. Jang, H.C. Son, P.H. Borse, J.S. Lee, Photocatalytic hydrogen production from natural seawater, J. Photochem. Photobiol., A 189 (2007) 141–144.
[13] Y. Nakaoka, H. Katsumata, S. Kaneco, T. Suzuki, K. Ohta, Photocatalytic degradation of diazinon in aqueous solution by platinized TiO_2, Desalin. Water Treat. 13 (2010) 427–436.
[14] L. Jianhua, Y. Rong, L. Songmei, Preparation and characterization of the TiO_2–V_2O_5 photocatalyst with visible-light activity, Rare Met. 25 (2006) 636–642.
[15] Y.Z. Li, D.S. Hwang, N.H. Lee, S.J. Kim, Synthesis and characterization of carbon-doped titania and artificial solar light sensitive photocatalyst, Chem. Phys. Lett. 404 (2005) 25–29.
[16] X.H. Wang, J.G. Li, H.K. Amiyama, Y. Moriyoshi, T. Ishigaki, Wavelength-sensitive photocatalytic degradation of methyl orange in aqueous suspension over iron (III)-doped iO_2 nanopowders under UV and visible light irradiation, J. Phys. Chem. B 110 (2006) 6804–6809.
[17] V.R. Shinde, T.P. Gujar, C.D. Lokhande, R.S. Mane, S.H. Han, Mn doped and undoped ZnO films: A comparative structural, optical and electrical properties study, Mater. Chem. Phys. 96 (2006) 326–330.
[18] D.T. Phuong, N. Quoc Tuan, B.T.H. Linh, L.G. Hy, T.M. Cuong, T.T.K. Hoa, L.M. Cam, V.A. Tuan, Photocatalytic degradation of p-xylene over doped titania thin film, Desalin. Water Treat. 34 (2011) 246–250.
[19] Z. Ambrus, N. Balazs, T. Alapi, G. Wittmann, P. Sipos, A. Dombi, K. Mogyorosi, Synthesis, structure and photocatalytic properties of Fe (III)-doped TiO_2 prepared from $TiCl_3$, Appl. Catal., B 81 (2008) 27–37.
[20] D. Chatterjee, S. Dasgupta, Visible light induced photocatalytic degradation of organic pollutants, J. Photochem. Photobiol., C 6 (2005) 186–205.
[21] D. Chatterjee, A. Mahata, Photosensitized detoxification of organic pollutants on the surface modified TiO_2 semiconductor particulate system, Catal. Commun. 2 (2001) 1–3.
[22] Mst. Sh. Nahar, K. Hasegawa, Sh. Kagaya, Sh. Kuroda, Comparative assessment of the efficiency of Fe-doped TiO_2 prepared by two doping methods and photocatalytic degradation of phenol in domestic water suspensions, Sci. Technol. Adv. Mater. 8 (2007) 286–291.
[23] U.G. Akpan, B.H. Hameed, Parameters affecting the photocatalytic degradation of dyes using TiO_2-based photocatalysts: A review, J. Hazard. Mater. 170 (2009) 520–529.
[24] D.B. Hamal, K.J. Klabunde, Synthesis, characterization and visible light activity of new nanoparticle photocatalysts based on silver, carbon and sulfur-doped TiO_2, J. Colloid Interface Sci. 311 (2007) 514–522.
[25] H. Feng, L.E. Yu, M.H. Zhang, Ultrasonic synthesis and photocatalytic performance or metal ions doped TiO_2 catalysts under solar light irradiation, Mater. Res. Bull. 48 (2013) 672–681.
[26] N. Venkatachalam, M. Palanichamy, V. Murugesan, Sol–gel preparation and characterization of alkaline earth metal doped nano TiO_2: Efficient photocatalytic degradation of 4-chlorophenol, J. Mol. Catal. A: Chem. 273 (2007) 177–185.
[27] M.A. Behnajady, N. Modirshahla, M. Shokri, H. Elham, A. Zeininezhad, The effect of particle size and crystal structure of titanium dioxide nanoparticles on the photocatalytic properties, J. Environ. Sci. Health, Part A 43 (2008) 460–467.
[28] J. Araña, J.M. Doña-Rodríguez, D. Portillo-Carrizo, C. Fernández-Rodríguez, J. Pérez-Peña, O. González Díaz, J.A. Navío, M. Macías, Photocatalytic degradation of phenolic compounds with new TiO_2 catalysts, Appl. Catal., B 100 (2010) 346–354.
[29] J. Araña, A. Peña Alonso, J.M. Doña Rodríguez, G. Colón, J.A. Navío, J. Pérez Peña, FTIR study of photocatalytic degradation of 2-propanol in gas phase with different TiO_2 catalysts, Appl. Catal., B 89 (2009) 204–213.
[30] S.R. Patil, U.G. Akpan, B.H. Hameed, S.K. Samdarshi, A comparative study of the photocatalytic efficiency of Degussa P25, Qualigens, and Hombikat UV-100 in the degradation kinetic of Congo red dye, Desalin. Water Treat. 46 (2012) 188–195.
[31] S. Anandan, P. Sathish Kumar, N. Pugazhenthiran, J. Madhavan, P. Maruthamuthu, Effect of loaded silver nanoparticles on TiO_2 for photocatalytic degradation of Acid Red 88, Sol. Energy Mater. Sol. Cells 92 (2008) 929–937.
[32] H. Delasa, B. Serrano, M. Salaices, Photocatalytic Reaction Engineering, Springer, New York, NY, 2005, pp. 39–45.
[33] S. Suwanboon, P. Amornpitoksuk, A. Sukolrat, Dependence of optical properties on doping metal, crystallite size and defect concentration of M-doped ZnO nanopowders (M = Al, Mg, Ti), Ceram. Int. 37 (2011) 1359–1365.
[34] M.A. Behnajady, N. Modirshahla, R. Hamzavi, Kinetic study on photocatalytic degradation of C.I. Acid Yellow 23 by ZnO photocatalyst, J. Hazard. Mater. 133 (2006) 226–232.
[35] Y. Li, Sh. Peng, F. Jiang, G. Lu, Sh. Li, Effect of doping TiO_2 with alkaline-earth metal ions on its photocatalytic activity, J. Serb. Chem. Soc. 72 (2007) 393–402.
[36] S. Ahmed, M.G. Rasul, W.N. Martens, R. Brown, M.A. Hashib, Heterogeneous photocatalytic degradation of phenols in wastewater: A review on current status and developments, Desalination 26 (2010) 3–18.
[37] M.A. Behnajady, N. Mansoriieh, N. Modirshahla, M. Shokri, Influence of operational parameters and kinetics analysis on the photocatalytic reduction of Cr(VI) by immobilized ZnO, Environ. Technol. 33 (2012) 265–271.
[38] M.A. Behnajady, Sh. Yavari, N. Modirshahla, Investigation on adsorption capacity of TiO_2–P25 nanoparticles in the removal of a mono-azo dye from aqueous solution: A comprehensive isotherm analysis, Chem. Ind. Chem. Eng. Q (in press), doi: 10.2298/CICEQ120610105B.
[39] P.K. Dutta, A.K. Ray, V.K. Sharma, F.J. Millero, Adsorption of arsenate and arsenite on titanium dioxide suspensions, J. Colloid Interface Sci. 278 (2004) 270–275.